Check for updates

ADVANCING EARTH AND SPACE SCIENCE

JGR Space Physics

RESEARCH ARTICLE

10.1029/2021JA029450

Morphology of the Auroral Tail of Io, Europa, and Ganymede From JIRAM L-Band Imager

Alessandro Moirano[1], Alessandro Mura[1], Alberto Adriani[1], Vincent Dols[2], Bertrand Bonfond[3], Jack H. Waite[4,5], Vincent Hue[4], Jamey R. Szalay[6], Ali H. Sulaiman[7], Bianca M. Dinelli[8], Federico Tosi[1], Francesca Altieri[1], Andrea Cicchetti[1], Gianrico Filacchione[1], Davide Grassi[1], Alessandra Migliorini[1], Maria L. Moriconi[8], Raffaella Noschese[1], Giuseppe Piccioni[1], Roberto Sordini[1], Diego Turrini[1], Christina Plainaki[9], Giuseppe Sindoni[9], Stefano Massetti[1], Robert L. Lysak[10], Stavro L. Ivanovski[11], and Scott J. Bolton[4]

[1]Institute for Space Astrophysics and Planetology, National Institute for Astrophysics (INAF—IAPS), Rome, Italy, [2]Laboratory for Atmospheric and Space Physics, University of Colorado, Boulder, Boulder, CO, USA, [3]Space sciences, Technologies and Astrophysics Research Institute, LPAP, Université de Liège, Liège, Belgium, [4]Southwest Research Institute, San Antonio, TX, USA, [5]Department of Physics and Astronomy, University of Texas at San Antonio, San Antonio, TX, USA, [6]Department of Astrophysical Sciences, Princeton University, Princeton, NJ, USA, [7]Department of Physics and Astronomy, University of Iowa, Iowa City, IA, USA, [8]Institute of Atmospheric Sciences and Climate, National Research Council (CNR—ISAC), Bologna, Italy, [9]Italian Space Agency (ASI), Rome, Italy, [10]School of Physics and Astronomy, University of Minnesota, Minneapolis, MN, USA, [11]National Institute for Astrophysics, Astronomical Observatory of Trieste (INAF—OAT), Trieste, Italy

Key Points:

- Jovian InfraRed Auroral Mapper (JIRAM) revealed periodic bright increases in the footprint tails of Europa and Ganymede similar to the ones previously observed for Io
- The typical distance between the luminous sub-dots is the same for Io, Europa and Ganymede in both hemispheres within the JIRAM resolution
- The sub-dots appear to corotate with Jupiter

Supporting Information:

Supporting Information may be found in the online version of this article.

Correspondence to:

A. Moirano,
alessandro.moirano@inaf.it

Citation:

Moirano, A., Mura, A., Adriani, A., Dols, V., Bonfond, B., Waite, J. H., et al. (2021). Morphology of the auroral tail of Io, Europa, and Ganymede from JIRAM L-band imager. *Journal of Geophysical Research: Space Physics*, *126*, e2021JA029450. https://doi.org/10.1029/2021JA029450

Received 15 APR 2021
Accepted 6 AUG 2021

© 2021. The Authors.
This is an open access article under the terms of the Creative Commons Attribution License, which permits use, distribution and reproduction in any medium, provided the original work is properly cited.

Abstract Jupiter hosts intense auroral activity associated with charged particles precipitating into the planet's atmosphere. The Galilean moons orbiting within the magnetosphere are swept by the magnetic field: the resulting perturbation travels along field lines as Alfven waves, which are able to accelerate electrons toward the planet, producing satellite-induced auroral emissions. These emissions due to the moons, known as *footprints*, can be detected in various wavelengths (UV, visible, IR) outside the main auroral emission as multiple bright spots followed by *footprint tails*. Since 2016 the Juno spacecraft orbiting Jupiter has surveyed the polar regions more than 30 times at close distances. Onboard the spacecraft, the Jovian InfraRed Auroral Mapper (JIRAM) is an imager and spectrometer with an L-band imaging filter suited to observe auroral features at unprecedented spatial resolution. JIRAM revealed a rich substructure in the footprint tails of Io, Europa, and Ganymede, which appear as a trail of quasi-regularly spaced bright sub-dots whose intensity fades away along the emission trail as the spatial separation from the footprint increases. The fine structure of the Europa and Ganymede footprint tails is reported in this work for the first time. We will also show that the typical distance between subsequent sub-dots is the same for all three moons at JIRAM resolution in both hemispheres. In addition, the sub-dots observed by JIRAM are static in a frame corotating with Jupiter. A feedback mechanism between the ionosphere and the magnetosphere is suggested as a potential candidate to explain the morphology of the footprint tails.

1. Introduction

Jupiter hosts auroral activities with an intensity significantly greater than Earth and Saturn (Grodent, 2015). Such phenomena are associated with charged particles precipitating into the planetary atmosphere. The origin of such energetic particles, the magnetic field, and potentially the solar activity are all elements determining both the morphology and the intensity of the auroral emissions. Jupiter has a strong and extended magnetic field that stretches for about 60–100 R_J in the subsolar direction (R_J = 72,492 km is the Jovian equatorial radius). It is dominated by a plasma whose density in the magnetosphere can be as high as a few thousand particles per cm^{-3}, as reviewed by Thomas et al. (2004) and more recently by Bagenal and Dols (2020). The plasma is believed to be predominantly supplied by the volcanic activity of Io (Thomas et al., 2004). As Jupiter's magnetic field rotates faster than the orbit of the Galilean moons, the moons are continuously swept by the Jovian magnetic field and the corotating magnetospheric plasma. This interaction triggers an electromagnetic coupling of the plasma in the magnetosphere with the ionized portion

of Jupiter's atmosphere known as the ionosphere. One of the coupling modes is a perturbation known as Alfven waves (Acuña et al., 1981; Belcher et al., 1981; Neubauer, 1980) that travel along the magnetic field lines toward the ionosphere that, under certain conditions, can develop a parallel electric field, which accelerates electrons into the atmosphere (Damiano et al., 2019; Hess et al., 2010; Jones & Su, 2008; Lysak & Song, 2003) and eventually produces auroral emissions (Connerney & Satoh, 2000). These waves are partially reflected by plasma density gradients and inhomogeneities in the Alfven speed (Crary & Bagenal, 1997; Hess et al., 2010; Hinton et al., 2019) (i.e., at the ionospheres of the boundaries of the Io Plasma Torus), leading to multiple bounces between the hemispheres and potential nonlinear wave evolution (Jacobsen et al., 2007).

The auroral signature due to satellite-ionosphere coupling is usually referred to as a *footprint* (FP) and can be identified equatorward of the main auroral emission (Clarke et al., 2004; Grodent, 2015) as a series of bright spots followed by an extended *footprint tail* (FPT) of fading emission (see for example Clarke et al., 2002; Mura et al., 2018). The footprint of Io is the easiest to detect (Clarke et al., 1996; Connerney et al., 1993; Prangé et al., 1996) because of its brightness and the latitudinal gap of its emission from the main auroral emission. The footprints of Ganymede and Europa are harder to discern since they are embedded in and obscured by the auroral emission region, where auroral injection signatures affect the brightness of the footprint (Bonfond, 2012; Bonfond et al., 2017). As for the footprint of Callisto, only two tentative detections using the Hubble Space Telescope UV cameras have been reported so far (Bhattacharyya et al., 2018). Its footprint is expected to be fainter than the other three footprints (Saur et al., 2013). Moreover, Callisto's footprint overlaps the main auroral emission. Therefore detecting it appears unlikely even at high resolution. In over 4 years of Juno observations, the footprint of Callisto has never been observed. Due to the lack of such observations by JIRAM, which is currently providing the largest database of Jupiter auroral footprints with the best spatial resolution to date, we conclude that the observation of Callisto associated feature is an extremely rare event. Thus, past and future claims of detection should be addressed cautiously. Up to three individual spots have been identified by the Hubble Space Telescope in the far-UV band for the Io footprint (Bonfond et al., 2008) and multiple spots have also been identified for the Ganymede (Bonfond et al., 2013) and Europa (Bonfond et al., 2017) footprints. Their inter-spot distances follow systematic variations as a function of System III longitude of the satellite, which is related to its location relative to the plasma torus or plasma sheet. The spots appear to be related to either (a) Alfven waves coming directly from the satellite (the Main Alfven Wing or MAW), (b) Alfven waves after one reflection by a density gradient (the Reflected Alfven Wing or RAW), or (c) to electrons accelerated away from Jupiter in one hemisphere and precipitating into the opposite one (the Trans-hemispheric Electron Beam or TEB). The locations of these three auroral features of the footprints were modeled for the Io's case (Hinton et al., 2019) and the results were in close agreement with the observations made by Hubble (Bonfond et al., 2017).

Auroral emission from Jupiter can be detected in many different wavelength ranges: ultraviolet (Caldwell et al., 1992; Clark & Mc Cord, 1980; Dols et al., 1992; Grodent et al., 2006; Livengood et al., 1992; Skinner et al., 1984), visible (Clarke et al., 2004; Ingersoll et al., 1998; Vasavada et al., 1999), and infrared (Drossart et al., 1989; Trafton et al., 1989). The polar, highly elliptical orbit of the Juno spacecraft around Jupiter offers an unprecedented opportunity to periodically survey the polar regions at close distance (Bagenal et al., 2017): less than $1R_J$ from the 1-bar level when Juno is over the polar regions. Juno's payload comprises imagers at ultraviolet, visible, and infrared wavelengths. The Jovian InfraRed Auroral Mapper (JIRAM) onboard Juno is an imager and spectrometer. Its L-band imaging channel is designed to observe auroral emission in the polar regions (Adriani et al., 2014). In particular, the JIRAM L-band filter is designed to observe the region between 3.3 and 3.6 μm that includes relatively strong H_3^+ lines with optimum contrast against the sunlit planetary disk.

H_3^+ ions are relatively easy to produce in Jupiter's ionosphere (Miller et al., 2020; Wu et al., 2019). Precipitating electrons ionize molecular hydrogen producing the H_2^+ ion, which under the atmospheric conditions of most auroral processes almost immediately reacts with H_2 to form H_3^+ according to the reaction

$$H_2^+ + H_2 \rightarrow H_3^+ + H.$$

There is an excess of 1.74 eV of energy that is, retained as internal energy of the H_3^+ molecule and subsequently released as IR emission due to transitions from its rotational and vibrational states (Oka, 1980).

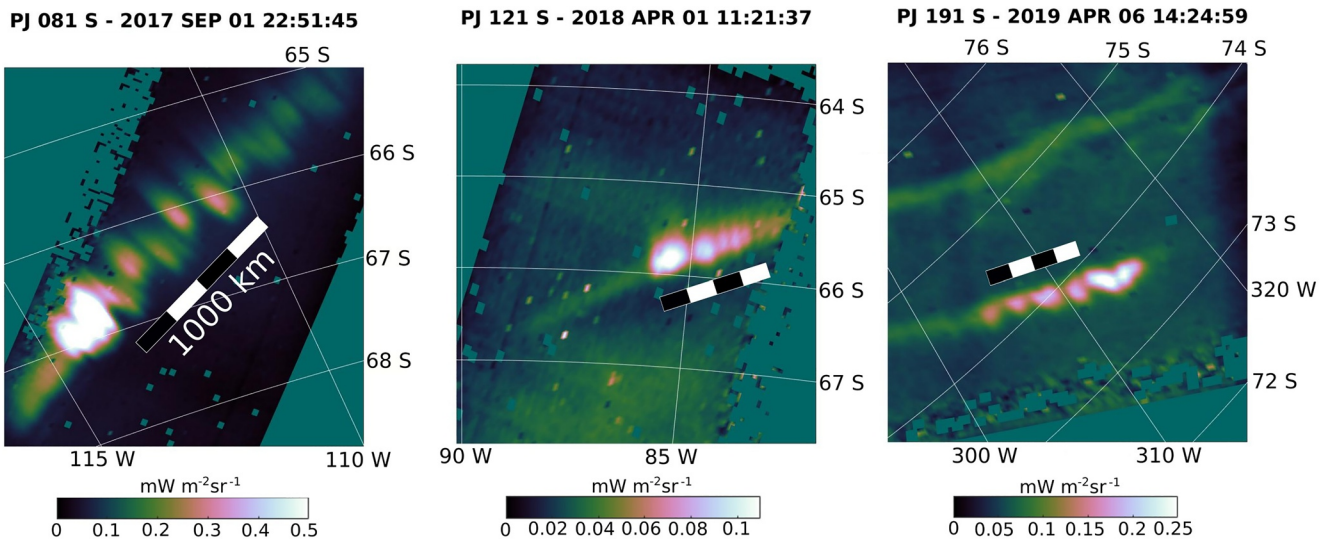

Figure 1. From left to right: examples of the Io, Europa, and Ganymede footprints and their dotted tails observed at the Southern pole during PJ 8, 12, and 19, respectively. The intensity is integrated over the bandwidth of the L-imager (3.3–3.6/*mu*m).

This emission depends also on the ionospheric conditions since collisions can repopulate rotational and vibrational states. The height of H_3^+ production is believed to peak at around 500–700 km (see Bonfond et al., 2009 for a discussion of the precise altitude of the emission of the Io footprint) dependent on the energy of the ionizing energetic particle and the altitude of the methane homopause. At altitudes below the methane homopause, the reaction with methane

$$H_3^+ + CH_4 \rightarrow CH_5^+ + H_2$$

efficiently prevents H_3^+ from radiating below the homopause, as the methane density rapidly increases with depth (Gérard et al., 2018).

The high spatial resolution of the imager (~0.01°, corresponding on average to a few tens of kilometers or less in Jupiter's ionosphere) provided the opportunity to discover a rich substructure in the Io footprint tail (Mura et al., 2018), which appears as a trail of staggered luminous dots whose brightness fades away down the tail. In order to avoid confusion between the aforementioned MAW-RAW-TEB spots and the fine structure we are focusing on, we will refer to the latter as *sub-dots*, as their size is smaller than the size of the MAW, RAW, and TEB spots. By surveying the JIRAM images from perijove (PJ) 4 to PJ 30 a similar morphology was also observed in the tails of Europa and Ganymede and reported for the first time in this work. In Figure 1 an example of the signature of each footprint is shown in System III reference frame (fixed with Jupiter magnetic field).

In Section 2, we report the data set of images used in the ensuing analyses as well as the data pre-processing we used. In Sections 3 and 4, we present two new results related to the observation of the footprint tail of Io, Europa, and Ganymede by JIRAM: the sub-dots corotate with Jupiter instead of following the footprint and the typical distance between the sub-dots in the tail is almost the same for all three moons at both hemispheres. In Section 5, we discuss previous observations of spot multiplicity in the footprint tails and their physical explanation. We then propose a feedback mechanism between the ionosphere and the magnetosphere as a potential explanation for the sub-dots in the footprint tails. We also briefly show images of the main auroral emission with a similar pattern as the sub-dots. In Section 6, we summarize our results.

2. Observations of the Footprint Tails

Images from the L-filter of JIRAM (which is a passband between 3.3 and 3.6 μm) are affected by the background interference from its M-filter (Mura et al., 2017), which is a passband between 4.5 and 5.0 μm designed to observe the jovian atmosphere (Adriani et al., 2014). In order to remove such an effect, we adopt

the empirical correction $A(x)e^{-y/B} + C$, where x and y are the columns and rows of the detector respectively ($y = 0$ is the row adjacent to the M-filter), while A, B, and C are evaluated for each image. Additional details regarding the algorithm, the calculation of A, B, and C for each image, and the data pipeline can be found in Mura et al. (2017). The correction for the interference helps the detection and study of the morphology of the auroral emissions, but slightly affects their observed intensity (Mura et al., 2018). The problem affects particularly the imager pixels near the junction to the M-band filter, where the correction gradually obscures all the emissions. For that reason, the pixels in the first 30 rows adjacent to the M-filter of each image are removed. The substructure in the Io footprint tail (IFPT) was immediately observed during the first orbits of Juno (Mura et al., 2018). On the other hand, the Europa and Ganymede footprints tails (EFPT and GFPT) are located within the equatorward edge of the auroral emissions region, therefore they can be obscured by its complex structure. Furthermore, planned observations of the Europa and Ganymede footprints (EFP and GFP, respectively) using the L-band filter are more likely to conflict with other scientific objectives of JIRAM, such as the observations of circumpolar cyclones (Adriani et al., 2018), while the observations in the area where the Io footprint (IFP) occurs do not compete with other scientific objectives. For these reasons, the substructure is more often observed in the IFPT than in the tail of the other moons.

Notwithstanding the small number of images acquired for each footprint, it is clear that the EFPT and GFPT can exhibit a detailed and rich structure similar to the one already observed in the IFPT. A morphologically rich sub-dots structure is almost always present in the IFPT and GFPT, while the EFPT occasionally appears as a fading auroral arc without evidence of any substructure. For this reason, we have a fewer number of observations where the Europa footprint shows sub-dots than in the case of the Ganymede footprint tail, even though the latter is closer to the main emission and thus more easily concealed by its activity. Indeed, JIRAM observed sub-dots in the EFPT during a single Juno pass over the northern hemisphere (PJ 20) and five over the southern one (PJ 12, 13, 14, 15, and 19), while sub-dots were observed for the GFPT during PJ 7 and 13 in the northern hemisphere and during PJ 7, 8, 11, 14, 16, 17, 18, 19, 20, 21, 27, 29, and 30 in the southern hemisphere.

The across-track size of the IFP perpendicular to the motion of the footprint is ~400 km, while the size of the EFP and GFP was ~300 km. This width is larger than the footprint size observed for Io from UV observations (<200 km (Bonfond, 2010)). Mapping this distance back to the orbits of the moons using the magnetic field model "Juno Reference Model through Perijove 9" (JRM09, Connerney et al., 2018), this width corresponds to an interaction region of about 3–4 satellite diameters (R_{Eu} = 1,560 km and R_{Ga} = 2,634 km). The external field due to the magnetodisk (Connerney et al., 1981) was not considered in mapping the size of the footprint to the ecliptic plane. The retrieved distance is slightly larger than the estimate of the interaction region at Io based on energetic electron measurements by JEDI during PJ 18 (Paranicas et al., 2019). The JEDI observations revealed electron depletion in a region of ~2.7 Io diameters wide perpendicular to its orbit. The same feature width was also observed at the same time in the JADE proton data when Juno was likely connected to the main Alfven wing (Szalay, Bagenal, et al., 2020).

3. Distance Between Sub-Dots

In this study, we consider images of the footprints acquired during the first 4 years of the Juno mission (~30 orbits). Although most of the images we used to analyze the morphology of the footprints were taken in the Southern hemisphere, JIRAM was able to capture at least one image of all three tail footprints in both hemispheres. The resolution of the images used in this work ranges between 15 and 55 km pixel^{-1} in the northern hemisphere, while it is between 40 and 110 km pixel^{-1} in the southern one. This wealth of high-spatial resolution data allows us to resolve a minimum distance of ~30–110 km and ~80–220 km between consecutive sub-dots in the two hemispheres, respectively.

For this estimation, we first select one image for each overflight on the polar regions (when available). Then the positions of the sub-dots are retrieved in each image as (X, Y, and Z) and the Euclidean distance d_i between them is evaluated for each pair of consecutive sub-dots. It is worth noticing that the difference between the Euclidean distance d_i and the spherical distance $D_i = \Delta\theta_i R_J$ is ~0.2 m for d_i ~ 300 km which is far smaller than the resolution of JIRAM (up to ~15–20 km pixel^{-1}). Therefore, we can consider the estimated Euclidean distance a good approximation of the spherical distance on Jupiter surface. For each

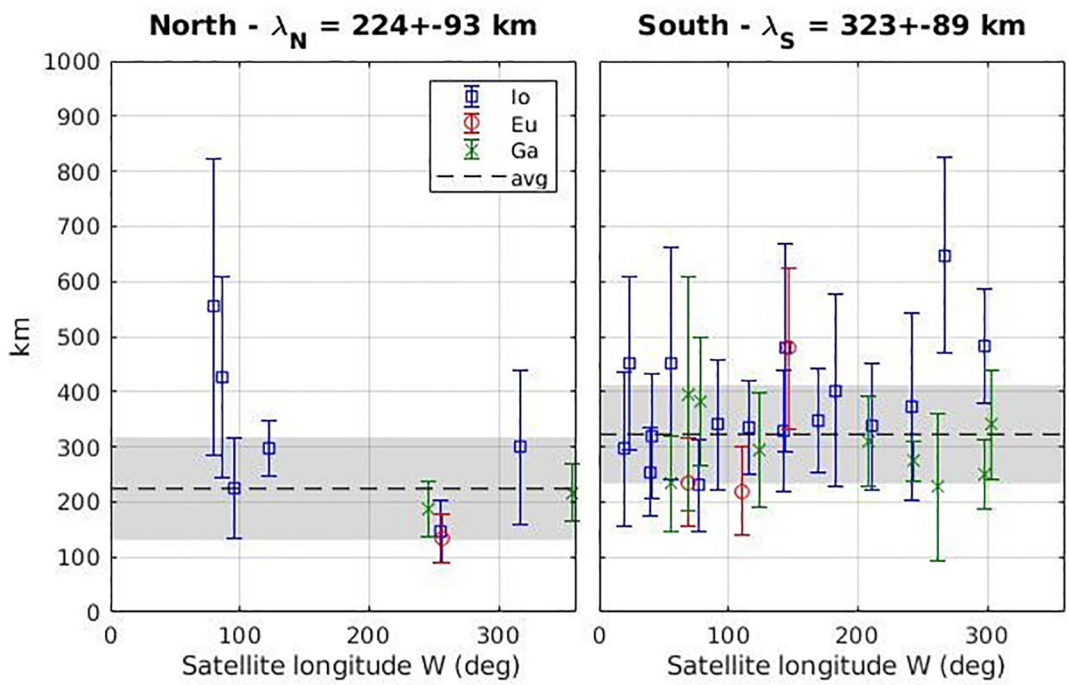

Figure 2. Average distance between sub-dots in the footprint tails of Io, Europa, and Ganymede for the northern and southern hemispheres (left and right, respectively). The dashed line is the statistically weighted average of the data points whose value is reported above each panel, while the gray area is the associated weighted standard deviation.

image we then retrieved the average distance $\langle d_i \rangle$ with associated standard deviation σ, which we used as uncertainty and thus it reflects the variability of the sub-dot distance in each image. The results are shown in Figure 2, where each data point corresponds to a retrieved value of $\langle d_i \rangle$. Finally, we computed the typical mean distance λ_{hemi} between the sub-dots by taking the average of $\langle d_i \rangle$ in each hemisphere, as indicated by the dashed lines in Figure 2.

In the northern hemisphere we found that the $\langle d_i \rangle$ varies from ~130–560 km and the average distance is $\lambda_N = 224 \pm 93$km. The shortest distance was observed when Io, Europa or Ganymede were around 250°W. This may suggest a potential longitudinal modulation of the sub-dot distance. In the southern hemisphere $\langle d_i \rangle$ varies mostly between 200 and 500 km, with an average $\lambda_S = 323 \pm 89$km.

Contrary to the behavior of the larger scale spots seen in the UV (Bonfond et al., 2017; Hinton et al., 2019), we found no clear evidence of modulation of the sub-dot distance with System III longitude of the footprints. Indeed, the distances between sub-dots in the IFPT in the right panel of Figure 2 was fitted by a sinusoidal function (not shown), so as to look for simple potential periodicities, but the residuals from the sinusoidal fit are worse than the residuals obtained from subtracting the average from the data set. The only evidence of variability is given by the three observations in the northern hemisphere near 250°W (left panel of Figure 2) when the distance fell below 200 km with relatively small uncertainty. This may be a localized feature at ~250° we found by chance or a suggestion that the modulation of the sub-dot distance is obscured by insufficient quality of the data to this purpose (as we already mentioned in Section 2, the L-band filter is affected by interference from the adjacent M-filter).

It is worth pointing out that the EFP and the GFP sometimes exhibit two bright spots separated by ~3,000 km. This distance is much larger than λ_N and λ_S: we suppose that they result from a different process than the spots shown in Figure 1 and therefore their distance was not included in Figure 2. As will be discussed in more detail in Section 5, this pair of spots can be explained by the bouncing of Alfven waves back and forth between the two hemispheres or by trans-hemispheric electron beams (Bonfond et al., 2008, 2013, 2017; Gérard et al., 2006), while the features of the trail of spots observed by JIRAM cannot. For this reason, we

will propose in Section 5 an ionosphere-magnetosphere feedback mechanism to explain the spot substructure as the underlying mechanism.

4. Dynamics of the Sub-Dots in the Footprint Tail

JIRAM was able to capture a continuous sequence of images of the IFP and its tail during the southern overflight of PJ 13 on May 24th 2018, from UTC 07:10:57 to 07:18:33. The imager acquired images ~30 s apart, which are shown in Figure 3 (animation of the same sequence can be found in the supporting information). During the sequence the IFP moved by about 3° westward, (from 67°W to 70°W), in about 7.5 min, with no displacement in latitude. The signature of the TEB that sometimes precedes the footprint (Bonfond et al., 2008) was not observed during the sequence in Figure 3. Indeed, the presence of the TEB ahead of the IFP and their relative position depend on the position of Io with respect to the centrifugal equator. At shown in Figure 3, Io was below the centrifugal equator, hence the TEB was not observed leading the IFP in agreement with previous observations and interpretations of the formation of the TEB (Bonfond et al., 2008; Hess et al., 2010).

The white arrow in Figure 3 outlines a specific sub-dot that appears to be in a stable position near 65°W in the corotating frame. In principle, the sampling frequency of the images can make the substructure of the tail appear static if, serendipitously, the sub-dots moved over the neighboring brightness trough in 30 s, which is the period between two consecutive images. The high resolution of the images allows us to observe and identify each separate sub-dot in different images. For example, the pair of sub-dots in Figure 3 highlighted by the blue arrows looks blended together and more extended, while the others between these two and the IFP are narrower and well separated from each other. This set of sub-dots was observed from 07:10:57 to 07:16:01 and it remained fixed slightly before 65°W. We are thus confident that the sub-dots in the tails are actually standing still in Jupiter's corotating frame and that this is not a result of the timing between images.

JIRAM captured two additional image series in the southern hemisphere which revealed the same behavior as the aforementioned one (PJ 14 and 26), even though the time windows covered were shorter (about 120 and 150 s, respectively). Hence, we believe that the stationary nature of the sub-dots in the rotating Jupiter frame observed during PJ 13 may be a consistent feature of the tail.

It is worth pointing out that in each panel of Figure 3 the sub-dots around 2,000 km down tail from the IFP (highlighted by the dotted circle) are brighter than the sub-dots right behind the footprint. Besides, this brightness envelope moves alongside the footprint, and the distance between the IFP and the envelope is of the same order of magnitude as the one between the spots in the EFPT and GFPT (~3,000 km). This suggests that the bouncing of Alfven waves is responsible for the two bright spots observed in the EFPT and GFPT as well as the intensity modulation of the sub-dots in the IFPT.

5. Discussion

Multiple spots were already observed in the footprint tail of Io. A bead-like tail that extends up to ~10° downstream of Io was observed and it was ascribed to bouncing of Alfven waves between the two hemispheres (Bonfond et al., 2008; Connerney & Satoh, 2000; Gérard et al., 2006; Hinton et al., 2019). Indeed, a precursor ahead of the footprint is sometimes observed, which is referred to as the Transhemispheric Electron Beam (TEB) (Bonfond et al., 2008). The EFP and GFP occasionally showed two bright spots, which can be also interpreted as reflections of Alfven waves or the result of the TEB (Bonfond et al., 2017). However, the sub-dots observed by JIRAM exhibit features that cannot be explained by the incidence of reflected Alfven waves. First, the pattern of the waves bouncing back and forth between the hemispheres is fixed in a frame corotating at the orbital period of the moon and gives a similar pattern to the spots (Jacobsen et al., 2007), while the structures observed by JIRAM are corotating with Jupiter. Secondly, the spots generated by the bouncing Alfven waves are separated by a few thousand kilometers (Bonfond et al., 2008; Gérard et al., 2006; Jacobsen et al., 2007), while sub-dots observed by JIRAM are separated by ~270± 90 km.

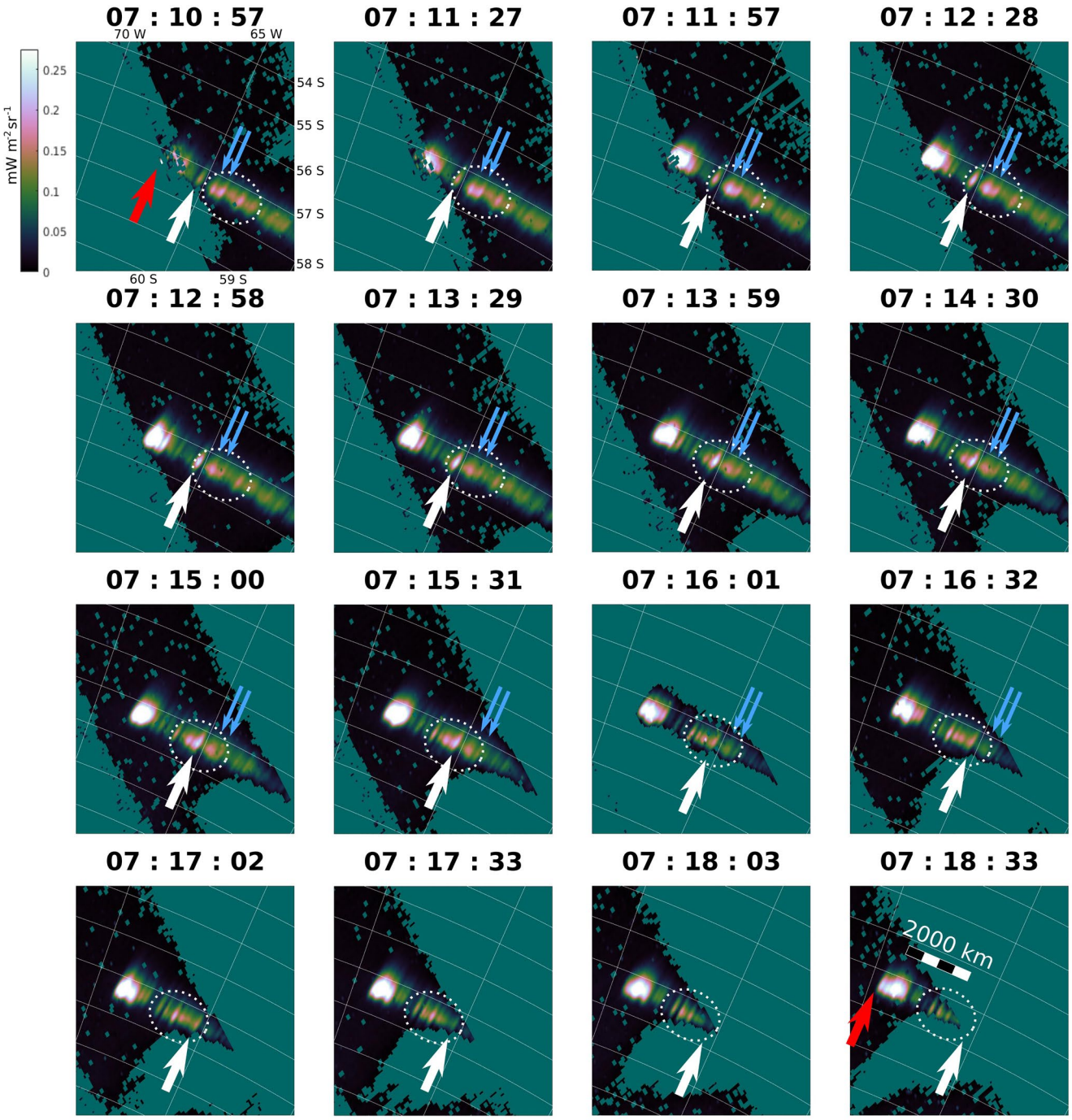

Figure 3. Sequence of images taken by Jovian InfraRed Auroral Mapper during PJ 13S from UTC 07:10:57 to 07:18:33. The red arrows point out the initial and final positions of the Io Footprint in the sequence, while the white and light blue arrows point out sample sub-dots that stayed near 65°W. The white dotted ellipses highlight a bright group of several sub-dots following the IFP at about 2,000 km. The intensity is integrated over the bandwidth of the L-imager (3.3–3.6 /*mu*m).

Finally, the inter-spot distance varies along the track of the footprint (the average distance is a few thousand kilometers) with the magnetic latitude of Io in the torus, while the distance between the sub-dots is observed by JIRAM did not show clear evidence of longitudinal variability.

Several hypotheses were proposed to explain the sub-dots in the IFPT (Mura et al., 2018). One of them suggested a local interaction between Io and the plasma torus. Indeed, a vortex street can form downstream of

Io as the plasma flows in a similar way as a von Karman vortex street in hydrodynamics (von Kármán, 1911). Alternatively, velocity shears in the radial direction in the low latitude magnetosphere near Io's orbit can also trigger Kelvin-Helmholtz instabilities (Chandrasekhar, 1961) and the subsequent formation of vortices. In both cases the underlying idea is that such vortices are then mapped onto the ionosphere, producing the observed pattern. Although these interpretations cannot be totally ruled out, it is unlikely that the prescribed triggering conditions take place in the environment of the Galilean moons. Indeed, the Kelvin-Helmholtz instability in magnetized plasmas requires a strong velocity shear as well as low magnetic tension along the flow direction (Chandrasekhar, 1961). The former is the source of energy for the development of the instability, while the latter slows down or can even completely suppress the process if there is no magnetic shear (otherwise the tearing mode instability is likely to help the Kelvin-Helmoltz instability to develop Chen et al., 1997; Ivanovski et al., 2011).

The corotating plasma near Io's orbit can be unstable to an azimuthal perturbation, which may lead to the formation of vortices (Hiraki et al., 2012) whose size is $\sim 0.5 R_J \approx 20 R_{Io}$. At the end of Section 2, we reported that the IFP size corresponds to about 3–4 Io diameters mapped onto the ionosphere along magnetic field lines, therefore it is unlikely that the emission associated with such vortices appears similar or smaller than the MAW spot. Kelvin-Heltmoltz vortices could potentially form on the flanks of Io due to the shear between its ionosphere and the flowing plasma of the IPT, similarly to the development of vortices on the flanks of the Earth's magnetosphere (Hasegawa et al., 2004). Assuming that the scale length of the shear layer is similar to the scale length of the density gradient in the ionosphere of Io (~200 km McElroy & Yung, 1975) and that the total velocity jump is given by the speed of Io relative to the plasma in the IPT (~60 km/s), then the growth rate is expected to be $\gamma \approx 0.01$–$0.03\ s^{-1}$ (Miura & Pritchett, 1982), depending on the compressibility of the plasma. Hence the sheared layer would require ~150–200 s (i.e., a few times γ^{-1} s) to evolve into a fully developed vortex sheet (Miura, 1997), which is not compatible with the observation of sub-dots immediately behind the main spot (see Figure 3). Furthermore, vortices can undergo nonlinear processes such as pairing and disruption (Miura, 1997) that should ultimately be reflected in the sub-dot appearance. The hydrodynamic von Karman vortex street develops only if the Reynolds number Re of the fluid (i.e., the ratio between inertia and viscosity) is in a certain range (Grenier, 2005). Because space plasmas usually have negligible viscosity, Re is usually very high and therefore turbulence is expected to develop in the wake of Io instead of a trail of vortices. Finally, the structure and dynamics of the vortices depend on the environmental parameters of each moon, as they determine the size of the shear layer, which in turn affects the most unstable mode. Each of the Galilean moons can interact electromagnetically with its surrounding plasma differently one from another (Saur et al., 2013) and their magnetic fields are different: these two elements potentially affect the size of the shear layer, which is unlikely to be the same for all three moons. So if the Kelvin-Heltmoltz instability triggers, the resulting vortices are likely to exhibit different morphologies, which is not consistent with the observations reported here.

Although vortices in the low latitude magnetosphere near the orbits of the Galilean moons are unlikely to develop or to exhibit features compatible with our observations (if they form), we want to underline that we cannot completely rule out the presence of vortices: further studies are needed to properly assess if vortices can develop as a result of the interaction of the moons with the magnetospheric plasma and what is their precise dynamics.

The feedback between the ionosphere and the magnetosphere may be the physical process underlying the trail of sub-dots we are discussing. The specific mechanism—sometimes referred to as the ionospheric feedback instability (IFI)—takes into account the effect of ionospheric changes on the magnetospheric circulation of field aligned currents (FACs) and is correlated with two factors: (a) the presence of a background ionospheric electric field and (b) a local increase of the ionospheric conductivity (Atkinson, 1970; Sato, 1978). Assuming a longitudinal arc-like region of increased conductivity and a transverse electric field related to the ionospheric current by $\vec{j}_I = \sigma \vec{E}_I$, the general picture of the feedback can be described as follows: the electric field of the Alfven wave enhances the ionospheric current, which then must be closed by additional field-aligned currents carried by secondary Alfven waves at the conductivity gradient. These waves can be reflected back toward the ionosphere at gradients in the Alfven speed such as the gradients in the topside ionosphere, the boundary of the plasma torus or the opposite ionosphere. This process leads to the structuring of the Alfven waves to scales at which the waves carry a parallel electric field that can

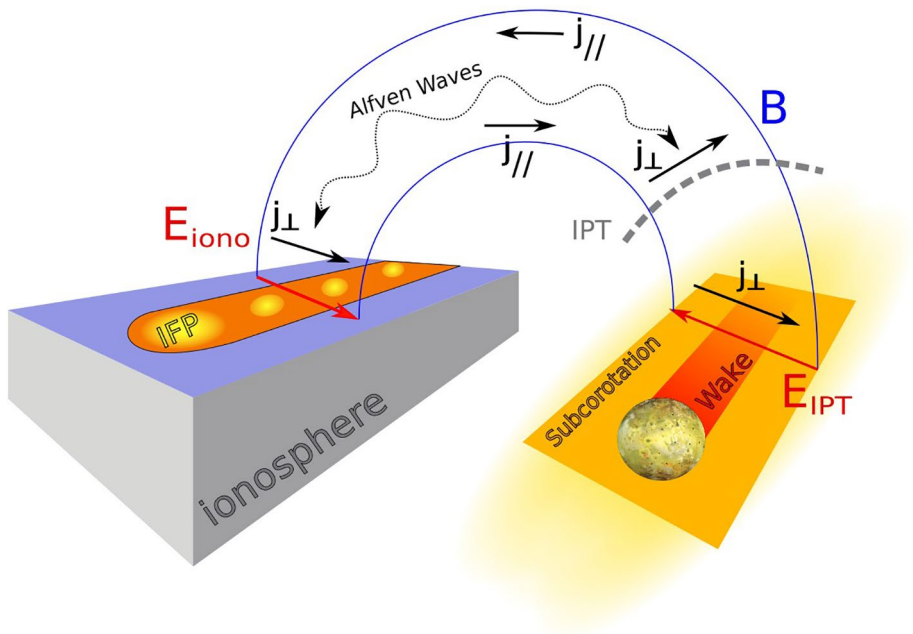

Figure 4. Sketch of the ionospheric feedback for the Io footprint in a frame corotating with Jupiter. The orange strip on the left represents the Io footprint tail and the yellow dots represent the sub-dots where the conductivity enhancement is expected, while the red and orange areas on the right represent the region where plasma is potentially sub-corotating. The red arrow is the electric field E_{IPT} associated to sub-corotation in the magnetosphere and mapped to E_{iono} at the ionosphere. The field aligned currents (black arrows) travel along the magnetic field (blue lines) carried by Alfven waves (dotted wavy arrow), which can be reflected by gradients in the Alfven velocity such as near the IPT (gray dashed line). The ionospheric feedback instability and the associated nonlinear evolution of the Alfven waves affect the Pedersen and Hall currents (not shown) as a consequence of the nonuniform conductivity in the ionosphere.

accelerate electrons, which then precipitate into the upper atmosphere producing ionization that further increases the conductivity and closes the feedback loop. This process goes on for as long as the flux tube crossed by the feedback waves can supply precipitating material. A qualitative sketch of the IFI is shown in Figure 4: the conductivity enhancement and the Alfvenic activity associated with the IFP affect the shape of the ionospheric currents (not shown), which in turn determines the morphology of the FACs. As a potential consequence, an alternating pattern of upward and downward currents can form along the IFPT, which should be reflected in the pattern of the auroral emission.

In the case of the Galilean moons, the conductivity enhancement is triggered by the precipitation associated with each footprint (Allegrini et al., 2020; Szalay et al., 2020a, 2020b). On the other hand, multiple factors can contribute to the background electric field. Generally, such an electric field can be provided by local subcorotation in the plasmasheet. Such corotation lag corresponds to a local magnetospheric electric field in the corotating frame, that, mapped along field lines into the jovian ionosphere, might provide the background electric field required for the instability. In the following paragraph, we briefly describe the observations and theoretical works that focus on subcorotation in the plasmasheet close to the Galilean moons: our goal is to provide qualitative support to the hypothesis of ionospheric feedback occurring along the footprint tails without delving into details. Voyager 1 and Galileo plasma observations were used to determine the azimuthal flow through the plasmasheet. although sometimes with quite large uncertainties. Bagenal et al. (2016) analyze Galileo PLS observations in the plasmasheet between 5 and 30 RJ and they conclude that the plasma flow begins to deviate from corotation near 9 RJ (close to Europa) and it is between 80% and 100% of corotation out to 25 RJ. Dougherty et al. (2017) re-analyze the Voyager plasma science data and they point out that the azimuthal flow starts to sub-corotate close to Europa, it dips down to 20% below corotation with a localized return to corotation at 17–20 RJ and reaches an asymptotic value of about 225 km/s further out. This corotation lag is due to the outward radial motion of the plasma in the plasmasheet. Indeed, the outward moving plasma slows down consistently with angular momentum conservation, but the presence of the planetary magnetic field couples the magnetosphere to the ionosphere, and hence angular

momentum is transferred from Jupiter to the plasmasheet. A stationary state, this process is mediated by a current loop that connects the plasmasheet and the jovian ionosphere along field lines and, as a consequence, the current flowing in the plasmasheet provides the $\vec{j} \times \vec{B}$ force that tends to accelerate the plasma toward corotation. Hill (1979) attributes the observed corotation lag to the Pedersen conductance which limits the current in the loop. Further refinements of this approach consider an increase of the Pedersen conductance provided by field-aligned currents (Nichols & Cowley, 2004) or the presence of field-aligned potential drops (Nichols & Cowley, 2005; Ray et al., 2010) and they suggest that the corotation should instead start to break at about 20–30 R_J. The discrepancy between observations and theoretical models will not be addressed in this work.

Beyond these general subcorotation trends, significant plasma slowing is also observed near the orbit of Io (Bagenal, 1985; Brown, 1983; Thomas et al., 2001). The plasma transport at Io is too small to cause the corotation lag, hence Pontius and Hill (1982) attribute this subcorotation to the ionization of neutral clouds of sulfur and oxygen that extend along Io's orbit (Brown, 1981; Durrance et al., 1983) by electron impact and charge exchange (Delamere & Bagenal, 2003). Ultimately, the ionospheric Pedersen conductance limits the ability of the current to restore the full corotation speed. In addition, dissipation in the magnetosphere-ionosphere coupling currents system may play an important role in the subcorotation near Io's orbit (Coffin et al., 2020).

At the moons themselves, the magnetospheric plasma is slowed in the wake of the moons by the pickup of newly ionized atmospheric neutrals at Io and Europa or by the interaction of the plasma with the intrinsic magnetic field of Ganymede. As a consequence, the magnetic field is stretched in the azimuthal direction and drives a radial current $\nabla \times \vec{B} = \mu_0 \vec{j}$ (Ergun et al., 2009). Corotation is then restored by the $\vec{j} \times \vec{B}$ force over time, so the electric field due to the wake is more important near the footprints than far downtail. Using numerical simulations of the plasma atmosphere interaction at Io and Europa, Saur et al. (1998) estimate that the flow is slowed by 95% at Io and 80% at Europa (see also Saur et al., 2013), thus the electric field in the wake may depend on the strength of the interaction between each moon and its environment.

The feedback between the ionosphere and magnetosphere described above has been previously studied on Earth because it could play a role in structuring the FACs and the auroral arcs (Miura & Sato, 1980; Streltsov & Mishin, 2018). Lysak and Song (2002) numerical analysis of the IFI indicated that this instability may play an important role in the formation of small-scale auroral arcs. Simulations also show that the active feedback of the auroral ionosphere on magnetic field-aligned currents carried by ULF Alfvén waves is able to describe different kinds of auroral structures (Jia & Streltsov, 2014). Indeed, the spatial and temporal behavior of the FACs producing the aurorae is strongly affected by the electric field and plasma parameters because of the highly nonlinear nature of the magnetosphere-ionosphere interaction. IFI was also related to the development of auroral vortex streets as a consequence of the coupling between the magnetospheric Alfvén waves carrying FACs and the ionospheric density waves driven by Pedersen and Hall currents (Hiraki, 2015). No reference to the application of this particular feedback mechanism to Jupiter was found in the literature. Nevertheless, there are qualitative arguments and order-of-magnitude estimates that support this feedback process in reproducing the morphology of the footprint tails.

First, the shear Alfven waves carry currents whose perpendicular components are aligned with the perpendicular wavevector (here and in the following *perpendicular* implies *perpendicular to the magnetic field*). At the ionosphere, these currents can affect the Hall and Pedersen currents, hence the evolution of the IFI ultimately depends on the relative direction between the ionospheric electric field $\vec{E}_I$ and the perpendicular wavevector $\vec{k}_\perp$ of the incident shear Alfven wave. Most of the theoretical studies of the IFI focused on a 2D geometry in which $\vec{k}_\perp \parallel \vec{E}_I$: in this case, the feedback process could lead to the formation of parallel arcs at different latitudes (see for example the theoretical results by Atkinson, 1970; Miura & Sato, 1980; Pokhotelov, 2003 and the measurements reported by Lynch et al., 2015; Tulegenov & Streltsov, 2017), reminiscent of the Io tail splitting observed by Mura et al. (2018) far down the tail. In order to include an arbitrary direction of $\vec{k}_\perp$ a full 3D geometry have to be considered. Numerical simulations of terrestrial auroral arcs showed that the direction of the most unstable $\vec{k}_\perp$ depends on the Hall and Pedersen background currents and that oblique $\vec{k}_\perp$ can produce ripples along the arc, which resemble the sub-dot structure addressed in this work (Hiraki, 2015; Watanabe, 2010). At Jupiter, the conductivity gradient associated with the IFP is structured in both longitude and latitude, hence modes along the direction of the footprint could be excited and driven unstable. In the

nonlinear phase of the IFI, these ripples form an alternating pattern of upward and downward currents, which may explain the small scale morphology JIRAM is observing in the footprint tails of the Galilean moons.

Second, Earth-based simulations of the feedback instability show that the typical distance between spots depends on the most unstable wavevector $\vec{k}_\perp = 2\pi\lambda_\perp^{-1}$ (Hiraki, 2015), whose wavelength $\lambda_\perp$ is related to $\lambda_\parallel$ by $\lambda_\perp = \lambda_\parallel \frac{\delta B_\perp}{B}$. In deriving this equation critical balance was assumed from the magnetohydrodynamics turbulence theory (Saur et al., 2018). The spectrum of the magnetic field measured by MAG and Waves instruments onboard Juno at ~0.4R_J from the surface revealed that the parallel wavelength of the fluctuations ranges from ~20 to ~$10^{-3}R_J$ (Sulaiman et al., 2020). In order to perform an order of magnitude estimate, we assume that this spectrum is the same (or at least very similar) at the altitude where auroral emissions occur. Taking into account the long wavelength end of the spectrum (that is, the wavelenghts near $\lambda_\parallel \sim 20R_J$), its amplitude (~200 nT Gershman et al., 2019; Sulaiman et al., 2020) and the magnetic field at Jupiter's surface ($B \sim 10^6$nT Connerney et al., 2018), the perpendicular wavelength is ~280km, which is similar to the value of λ_N and λ_S we retrieved in Section 3. Dispersion of the Alfven waves due to inertial effects and mode trapping in the ionospheric cavity may need to be considered in order to better estimate $\lambda_\perp$, but the result from this approximate estimate alone is encouraging.

Furthermore, the periodic pattern in the nonlinear phase of the instability moves at a speed given by $\vec{E}_I \times \vec{B}$ drift (Atkinson, 1970; Hiraki, 2015; Watanabe, 2010). The electric field in the magnetosphere associated with the sub-corotation velocity $\Delta\vec{u}$ is given by $\vec{E}_M = \Delta\vec{u} \times \vec{B}_M$, where $\vec{B}_M$ is the magnetic field in the equatorial plane. In order to give a quantitative estimate, we take $\Delta\vec{u}$ from the corotation lag observed from ~ 10R_J outward for Europa and Ganymede (Dougherty et al., 2017), while for Io we considered the departure from corotation observed near 5.9R_J (Brown, 1983). Therefore, for Io, Europa and Ganymede the corotation lag is ~5%, ~10% and ~20% of the corotation velocity respectively. As a first approximation, the relationship between ionospheric and magnetospheric field is given by $\vec{E}_I = \beta\vec{E}_M$ if there is no potential drop along magnetic field lines (Ergun et al., 2009). The electric field and the consequent drift can be up to 50% lower if parallel potentials are generated along field lines, depending on the ionospheric and field-aligned conductances (Ergun et al., 2009). The mapping factor β stems from the conservation of magnetic flux between the moons and the ionosphere of Jupiter assuming that field lines are equipotentials. Considering a flux tube of radius R_M at the ecliptic and R_I at the ionosphere, the potential drop ΔV across the flux tube must be the same along the tube itself, therefore $\Delta V \approx E_M R_M \approx E_I R_I$ and thus $\beta \approx R_M / R_I$. Taking typical values $\beta \approx 30$ and $|\vec{B}| \approx 10^6$nT, then $|\vec{E}_I| \approx 0.1 - 0.2$V/m and $v_{drift} \approx 0.1 - 0.2$km/s in a frame corotating with Jupiter, which is much slower than the speed of the footprints (usually between 2.5 and 4 km/s). Consequently, the structure of the whole tail would move by about 3–6 km in between consecutive JIRAM images and by 45–90 km during the whole sequence in Figure 3. The resolution of the images was between 70 and 80 km per pixel at the times in Figure 3, so the sub-dots would move the length of one pixel at maximum because of the drift. Therefore, this velocity is consistent with the apparent stationary nature of the sub-dots in Jupiter's frame observed by JIRAM.

Evidence of dot-like structures with wavelengths similar to those observed in the footprint tails were also detected along the main emission. Examples of such observations can be seen in Figure 5. The morphology appears less regular than the footprint tail, but the brightness is not uniform and luminous sub-dots appear quasi-regularly spaced along the arc. The mean retrieved distance between sub-dots of the two examples in Figure 5 is higher than the ones in Figure 2, but it is compatible with them within the uncertainty. This suggests that the morphology observed in the footprint tails may be caused by an ionospheric process that is, not exclusive of the satellite-ionosphere coupling, even though the interaction between the moons and the planetary magnetic field plays a crucial role in triggering the alfvenic perturbation. Alternatively, the pattern observed along the main emission may be due to variation in the electron flux impinging on the ionosphere (Watanabe et al., 2018). The qualitative description and the distribution of the feature in Figure 5 over Jupiter are outside the scope of this work and will be addressed in a separate work.

As discussed in Section 2, the EFPT often shows a continuous arc instead of a trail of sub-dots. This might be caused by the fact that the conditions for the IFI to develop are not always met for the Europa case, meaning that the increase of ionospheric conductivity is too low or that the ionospheric electric field is too weak. The electrodynamical interaction at Europa with its surroundings is weaker than at Io and Ganymede (Saur

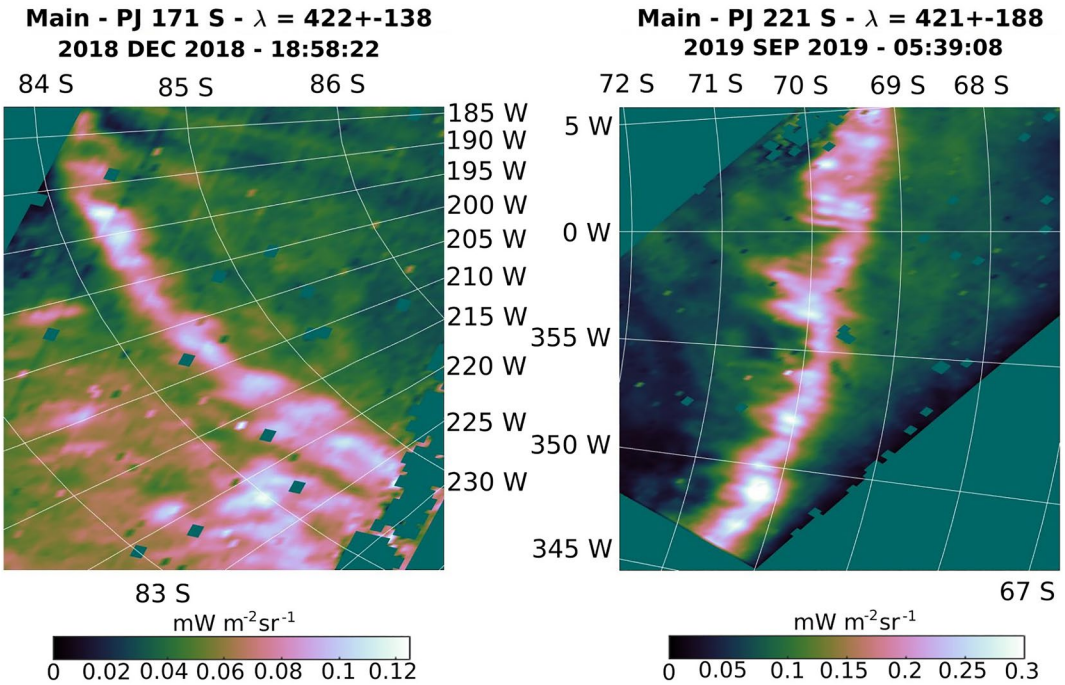

Figure 5. Images of the main emission showing local enhancements of brightness in the Southern hemispheres. The morphology of the main emission is not as regular as the one of the footprint tails, but it shows some periodicity. The intensity is integrated over the bandwidth of the L-imager (3.3–3.6/*mu*m).

et al., 2013). Indeed, the volcanic activity of Io generates an ionosphere that interacts with the surrounding dense plasma of the Io plasma torus, while the intrinsic magnetic field of Ganymede diverts impinging plasma and makes this moon a bigger obstacle than its solid cross section suggests (Saur et al., 2013). Thus the weak interaction at Europa can affect the ionospheric electric field at Jupiter and perhaps the conductivity as a consequence of electron precipitation so that the IFI cannot be triggered. Nevertheless, JIRAM occasionally observed a trail of sub-dots in the EFPT. This may occur when Europa is in particular environmental conditions such as plasma sheet crossing, water outgassing (Paganini et al., 2020; Roth et al., 2014), or plasma injections (Mauk et al., 1997) so that the interaction becomes temporarily strong enough to trigger the IFI.

Nevertheless, the feedback mechanism needs to be further investigated. The feedback itself structures the field-aligned currents/Alfven waves so that they develop the parallel electric field that can accelerate the electrons (Hess et al., 2010; Lysak & Song, 2003). Since this mechanism depends on the ionospheric parameters and not on the moons themselves, this might be the reason that the spot spacing is similar for all three moons. Nevertheless, the relation between the ionospheric current system generated by the IFI and the electric field in the acceleration region needs to be addressed quantitatively to estimate the intensity of the auroral emission (Hiraki, 2015).

Furthermore, Earth-based simulations reveal that the growth rate and the most unstable mode of the IFI depend on the Pedersen and Hall conductances in the ionosphere (Watanabe, 2010) and on the magnitude of the background electric field (Hiraki, 2015). These two pieces of information are fundamental to carry out a proper quantitative comparison between the observations made by JIRAM and the feedback model and will require further analysis to properly determine.

Moreover, the role of the ionospheric Alfven resonator (IAR), a resonant cavity caused by the sharp gradient in the Alfven speed above the ionosphere, can affect the development of the IFI. Indeed, the IFI can be triggered by eigenmodes of field line resonances extending from one ionosphere to the other (e.g., Rankin et al., 2005), as well as by eigenmodes of the IAR (Lysak, 1991; Pokhotelov et al., 2001): the former drives a slow IFI with periods of a few minutes while the latter drives a fast IFI with periods of a few seconds (Lysak

& Song, 2002). There have been no published reports of the application of this feedback mechanism in the Jovian magnetosphere. However, at Jupiter, there is also the possibility of feedback in the cavity formed in the high Alfvén speed region between the ionosphere and the Io plasma torus. The interplay of these various cavities may affect the morphology and brightness of the footprint tails due to the different time scales of these cavities.

Regarding the energy budget of the feedback process, Earth-based simulations reveal that the energy of the Alfven waves leaving the ionosphere is correlated to the decrease of Joule heating, which results from the increased ionospheric conductivity (Lysak & Song, 2002). In addition, infrared H_3^+ auroral emissions on Jupiter are mostly due to chemical reactions (Grodent, 2015; Miller et al., 2020), which may strongly damp the IFI (Lysak & Song, 2002). Therefore, the relationship between the energetics of the IFI and the intensity of the IR emission is not straightforward and requires further investigation.

6. Conclusion

In this paper, we analyzed images of the footprint of Io, Europa, and Ganymede taken by the L-band filter of JIRAM during the first 30 orbits of Juno. The major findings we reported can be summarized as follow:

1. The footprint tails of Europa and Ganymede show a small scale morphology similar to the one previously observed in the Io footprint tail (Mura et al., 2018), although the footprint tail of Europa occasionally shows up as a fading auroral arc without evidence of any substructure.
2. The typical distance between the sub-dots observed by JIRAM is ~270 ± 90 km. This distance is the same for all three moons at both hemispheres within the uncertainty.
3. The sub-dots were observed to corotate with Jupiter during the sequence of images taken during PJ 13 when JIRAM followed the footprint of Io for about 8 min. Shorter series showing the same behavior were also acquired during PJ 14 and 26, which suggest that this dynamics is consistent.

We propose that the small scale morphology reported in this work may be caused by a feedback mechanism between the ionosphere and the magnetosphere, also called ionospheric feedback instability (Atkinson, 1970; Sato, 1978). This process triggers where an ionospheric current flows across a local increase of conductance: in this scenario, the increased ionospheric current is closed at the conductivity gradient by secondary field aligned currents carried by Alfven waves. Such waves can be reflected by gradients in the Alfven speed and accelerate electrons while they travel back, thus leading to a further increase in the ionospheric conductance. The feedback instability has been previously investigated as it could affect the structure of the field aligned current and the auroral arcs on Earth and no reference of application to Jupiter were found in the literature. In the case of the footprint tails, the associated electron precipitation causes the local conductivity enhancement, while the currents could be generated by corotation lag in the plasmasheet (for Europa and Ganymede), by local subcorotation in the IPT (for Io), or by the electric field generated in the wakes of the satellites.

We proposed qualitative arguments and order of magnitude estimates that can support the feedback process as a potential explanation to the sub-dots reported in this work. We summarize our conclusions:

1. Three dimensional simulation of the feedback instability on Earth showed the auroral arc can evolve into a vortex street (Hiraki, 2015; Watanabe, 2010). The specific morphology of the currents driven by the instability depends on the intensity of the ionospheric electric field and the direction of the wavevector of the incident Alfven wave with respect to the auroral arc.
2. The perpendicular wavelength of the magnetic field fluctuations measured by MAG onboard Juno (Gershman et al., 2019; Sulaiman et al., 2020) are compatible with the observed distance between the sud-dots.
3. The vortex street generated by the instability moves at a speed given by the $\vec{E} \times \vec{B}$ drift (Hiraki, 2015). If the electric field is inferred from subcorotation (Ergun et al., 2009), then the drift speed is consistent with the apparent stationary nature of the sub-dots we reported.
4. Dot-like features similar to the one observed in the footprint tails are also observed along the main auroral emission. Although these structures show a less regular morphology, they might be caused by an ionospheric process that is, not exclusive of the satellite-ionosphere coupling.

The feedback mechanism needs further studies in order to answer additional questions:

1. The parallel electric field developed by the Alfven waves is likely to accelerate electrons along the field lines (Hess et al., 2010; Lysak & Song, 2003), therefore the IFI may potentially affect the brightness of the sub-dots as well as the tail extent, although this aspect needs to be further investigated.
2. The growth rate and the unstable modes depend on the Hall and Pedersen conductivities as well as on the ionospheric electric field (Hiraki, 2015): both are fundamental to perform a proper quantitative analysis.
3. We did not consider the role of the ionospheric resonator (Lysak, 1991) for sake of simplicity, but the fast feedback that can be triggered here should be taken into account for a proper quantitative investigation.
4. Relating the energy budget of the feedback instability (which relies on the decrease of Joule heating in the ionosphere; Lysak & Song, 2002) to the observed intensity of the IR emission (which depends on the emission of the H_3^+ ion) is not straightforward and requires additional investigation.

Data Availability Statement

Data and materials availability: JIRAM data used in this study is publicly available on the Planetary Data System (http://pds.nasa.gov). Repository for the data products used in this study is: https://doi.org/10.5281/zenodo.4687920.

Acknowledgments
The authors thank Agenzia Spaziale Italiana (ASI) for support of the JIRAM contribution to the Juno mission (JIRAM is funded with ASI contract 2016-353 23-H.0). Open access funding enabled and organized by Projekt DEAL.

References

Acuña, M. H., Neubauer, F. M., & Ness, N. F. (1981). Standing Alfvén wave current system at Io: Voyager 1 observations. *Journal of Geophysical Research*, *86*(A10), 8513–8521. https://doi.org/10.1029/JA086iA10p08513

Adriani, A., Filacchione, G., Di Iorio, T., Turrini, D., Noschese, R., Cicchetti, A., et al. (2014). JIRAM, the Jovian infrared auroral mapper. *Space Science Reviews*, *213*(1–4), 393–446. https://doi.org/10.1007/s11214-014-0094-y

Adriani, A., Mura, A., Orton, G., Hansen, C., Altieri, F., Moriconi, M. L., et al. (2018). Clusters of cyclones encircling Jupiter's poles. *Nature*, *555*(7695), 216–219. https://doi.org/10.1038/nature25491

Allegrini, F., Gladstone, G. R., Hue, V., Clark, G., Szalay, J. R., Kurth, W. S., et al. (2020). First report of electron measurements during a Europa footprint tail crossing by Juno. *Geophysical Research Letters*, *47*(18), e2020GL089732. https://doi.org/10.1029/2020GL089732

Atkinson, G. (1970). Auroral arcs: Result of the interaction of a dynamic magnetosphere with the ionosphere. *Journal of Geophysical Research*, *75*(25), 4746–4755. https://doi.org/10.1029/JA075i025p04746

Bagenal, F. (1985). Plasma conditions inside Io's orbit: Voyager measurements. *Journal of Geophysical Research*, *90*(A1), 311–324. https://doi.org/10.1029/JA090iA01p00311

Bagenal, F., Adriani, A., Allegrini, F., Bolton, S. J., Bonfond, B., Bunce, E. J., et al. (2017). Magnetospheric science objectives of the Juno mission. *Space Science Reviews*, *213*(1–4), 219–287. https://doi.org/10.1007/s11214-014-0036-8

Bagenal, F., & Dols, V. (2020). The space environment of Io and Europa. *Journal of Geophysical Research: Space Physics*, *125*(5), e2019JA027485. https://doi.org/10.1029/2019JA027485

Bagenal, F., Wilson, R. J., Siler, S., Paterson, W. R., & Kurth, W. S. (2016). Survey of Galileo plasma observations in Jupiter's plasma sheet. *Journal of Geophysical Research: Planets*, *121*(5), 871–894. https://doi.org/10.1002/2016JE005009

Belcher, J. W., Goertz, C. K., Sullivan, J. D., & Acuña, M. H. (1981). Plasma observations of the Alfvén wave generated by Io. *Journal of Geophysical Research*, *86*(A10), 8508–8512. https://doi.org/10.1029/JA086iA10p08508

Bhattacharyya, D., Clarke, J. T., Montgomery, J., Bonfond, B., Gérard, J., & Grodent, D. (2018). Evidence for auroral emissions from Callisto's Footprint in HST UV Images. *Journal of Geophysical Research: Space Physics*, *123*(1), 364–373. https://doi.org/10.1002/2017JA024791

Bonfond, B. (2010). The 3-D extent of the Io UV footprint on Jupiter. *Journal of Geophysical Research*, *115*(A9). https://doi.org/10.1029/2010JA015475

Bonfond, B. (2012). When moons create aurora: The satellite footprints on giant planets. In A. Keiling, E. Donovan, F. Bagenal, & T. Karlsson, T. (Eds.), *Auroral phenomenology and magnetospheric processes: Earth and other planets* (pp. 133–140). American Geophysical Union (AGU). https://doi.org/10.1029/2011GM001169

Bonfond, B., Grodent, D., Badman, S. V., Saur, J., Gérard, J. C., & Radioti, A. (2017). Similarity of the Jovian satellite footprints: Spots multiplicity and dynamics. *Icarus*, *292*, 208–217. https://doi.org/10.1016/j.icarus.2017.01.009

Bonfond, B., Grodent, D., Gérard, J.-C., Radioti, A., Dols, V., Delamere, P. A., & Clarke, J. T. (2009). The Io UV footprint: Location, inter-spot distances and tail vertical extent. *Journal of Geophysical Research*, *114*, A07224. https://doi.org/10.1029/2009JA014312

Bonfond, B., Grodent, D., Gérard, J.-C., Radioti, A., Saur, J., & Jacobsen, S. (2008). UV Io footprint leading spot: A key feature for understanding the UV Io footprint multiplicity? *Geophysical Research Letters*, *35*(5), L05107. https://doi.org/10.1029/2007GL032418

Bonfond, B., Hess, S., Bagenal, F., Gérard, J.-C., Grodent, D., Radioti, A., et al. (2013). The multiple spots of the Ganymede auroral footprint. *Geophysical Research Letters*, *40*(19), 4977–4981. https://doi.org/10.1002/grl.50989

Brown, R. A. (1981). The Jupiter hot plasma torus—Observed electron temperature and energy flows. *Acta Pathologica Japonica*, *244*, 1072. https://doi.org/10.1086/158777

Brown, R. A. (1983). Observed departure of the Io plasma torus from rigid corotation with Jupiter. *The Astrophysical Journal*, *268*, L47. https://doi.org/10.1086/184027

Caldwell, J., Turgeon, B., & Hua, X.-M. (1992). Hubble space telescope imaging of the North Polar Aurora on Jupiter. *Science*, *257*(5076), 1512–1515. https://doi.org/10.1126/science.257.5076.1512

Chandrasekhar, S. (1961). *Hydrodynamic and hydromagnetic stability*. Courier Corporation.

Chen, Q., Otto, A., & Lee, L. C. (1997). Tearing instability, Kelvin-Helmholtz instability, and magnetic reconnection. *Journal of Geophysical Research*, *102*(A1), 151–161. https://doi.org/10.1029/96JA03144

Clarke, J. T., Ajello, J., Ballester, G., Ben Jaffel, L., Connerney, J., Gérard, J.-C., et al. (2002). Ultraviolet emissions from the magnetic footprints of Io, Ganymede and Europa on Jupiter. *Nature*, *415*(6875), 997–1000. https://doi.org/10.1038/415997a

Clarke, J. T., Ballester, G. E., Trauger, J., Evans, R., Connerney, J. E. P., Stapelfeldt, K., et al. (1996). Far-ultraviolet imaging of Jupiter's aurora and the Io "Footprint". *Science*, *274*(5286), 404–409. https://doi.org/10.1126/science.274.5286.404

Clarke, J. T., Grodent, D., Cowley, S. W. H., Bunce, E. J., Zarka, P., Connerney, J. E. P., & Satoh, T. (2004). Jupiter's Aurora. In *Jupiter: The Planet, Satellites and magnetosphere* (Vol. 1, pp. 639–670). Cambridge University Press.

Clark, R. N., & Mc Cord, T. B. (1980). The Galilean satellites: New near-infrared spectral reflectance measurements (0.65–2.5 m) and a 0.325–5 m summary. *Icarus*, *41*(3), 323–339. https://doi.org/10.1016/0019-1035(80)90217-1

Coffin, D., Delamere, P., & Damiano, P. (2020). Implications for magnetosphere-ionosphere coupling from Jupiter's system IV Quasi-Period. *Journal of Geophysical Research: Space Physics*, *125*(5), e2019JA027347. https://doi.org/10.1029/2019JA027347

Connerney, J. E. P., Acuña, M. H., & Ness, N. F. (1981). Modeling the Jovian current sheet and inner magnetosphere. *Journal of Geophysical Research*, *86*(A10), 8370–8384. https://doi.org/10.1029/JA086iA10p08370

Connerney, J. E. P., Baron, R., Satoh, T., & Owen, T. (1993). Images of excited H_3^+ at the foot of the Io Flux tube in Jupiter's atmosphere. *Science*, *262*(5136), 1035–1038. https://doi.org/10.1126/science.262.5136.1035

Connerney, J. E. P., Kotsiaros, S., Oliversen, R. J., Espley, J. R., Joergensen, J. L., Joergensen, P. S., et al. (2018). A new model of Jupiter's magnetic field from Juno's first nine orbits. *Geophysical Research Letters*, *45*(6), 2590–2596. https://doi.org/10.1002/2018GL077312

Connerney, J. E. P., & Satoh, T. (2000). The H+3 ion: A remote diagnostic of the Jovian magnetosphere. *Philosophical Transactions: Mathematical, Physical and Engineering Sciences*, *358*(1774), 2471–2483. https://doi.org/10.1098/rsta.2000.0661

Crary, F. J., & Bagenal, F. (1997). Coupling the plasma interaction at Io to Jupiter. *Geophysical Research Letters*, *24*(17), 2135–2138. https://doi.org/10.1029/97GL02248

Damiano, P. A., Delamere, P. A., Stauffer, B., Ng, C.-S., & Johnson, J. R. (2019). Kinetic simulations of electron acceleration by dispersive scale Alfvén waves in Jupiter's magnetosphere. *Geophysical Research Letters*, *46*(6), 3043–3051. https://doi.org/10.1029/2018GL081219

Delamere, P. A., & Bagenal, F. (2003). Modeling variability of plasma conditions in the Io torus. *Journal of Geophysical Research*, *108*(A7), 1276. https://doi.org/10.1029/2002JA009706

Dols, V., Gérard, J. C., Paresce, F., Prangé, R., & Vidal-Madjar, A. (1992). Ultraviolet imaging of the Jovian aurora with the Hubble Space Telescope. *Geophysical Research Letters*, *19*(18), 1803–1806. https://doi.org/10.1029/92GL02104

Dougherty, L. P., Bodisch, K. M., & Bagenal, F. (2017). Survey of Voyager plasma science ions at Jupiter: 2. Heavy ions. *Journal of Geophysical Research: Space Physics*, *122*(8), 8257–8276. https://doi.org/10.1002/2017JA024053

Drossart, P., Maillard, J., Caldwell, J., Kim, S., Watson, J., Majewski, W., et al. (1989). Detection of H_3^+ on Jupiter. *Nature*, *340*, 539–541. https://doi.org/10.1038/340539a0

Durrance, S. T., Feldman, P. D., & Weaver, H. A. (1983). Rocket detection of ultraviolet emission from neutral oxygen and sulfur in the Io Torus. *Acta Pathologica Japonica*, *267*, L125. https://doi.org/10.1086/184016

Ergun, R. E., Ray, L., Delamere, P. A., Bagenal, F., Dols, V., & Su, Y.-J. (2009). Generation of parallel electric fields in the Jupiter-Io torus wake region. *Journal of Geophysical Research*, *114*(A5), A05201. https://doi.org/10.1029/2008JA013968

Gérard, J.-C., Mura, A., Bonfond, B., Gladstone, G., Adriani, A., Hue, V., et al. (2018). Concurrent ultraviolet and infrared observations of the north Jovian aurora during Juno's first perijove. *Icarus*, *312*, 145–156. https://doi.org/10.1016/j.icarus.2018.04.020

Gérard, J.-C., Saglam, A., Grodent, D., & Clarke, J. T. (2006). Morphology of the ultraviolet Io footprint emission and its control by Io's location. *Journal of Geophysical Research*, *111*(A4), A04202. https://doi.org/10.1029/2005JA011327

Gershman, D. J., Connerney, J. E. P., Kotsiaros, S., DiBraccio, G. A., Martos, Y. M., Viñas, A. F., et al. (2019). Alfvénic fluctuations associated with Jupiter's auroral emissions. *Geophysical Research Letters*, *46*(13), 7157–7165. https://doi.org/10.1029/2019GL082951

Grenier, E. (2005). Chapter 4—Boundary layers. In S. Friedlander, & D. Serre (Eds.), *Handbook of Mathematical fluid dynamics* (Vol. 3, pp. 245–309). North-Holland. https://doi.org/10.1016/S1874-5792(05)80007-2

Grodent, D. (2015). A brief review of ultraviolet auroral emissions on giant planets. *Space Science Reviews*, *187*(1–4), 23–50. https://doi.org/10.1007/s11214-014-0052-8

Grodent, D., Gérard, J.-C., Gustin, J., Mauk, B. H., Connerney, J. E. P., & Clarke, J. T. (2006). Europa's FUV auroral tail on Jupiter. *Geophysical Research Letters*, *33*(6), L06201. https://doi.org/10.1029/2005GL025487

Hasegawa, H., Fujimoto, M., Phan, T.-D., Rème, H., Balogh, A., Dunlop, M. W., et al. (2004). Transport of solar wind into Earth's magnetosphere through rolled-up Kelvin-Helmholtz vortices. *Nature*, *430*(7001), 755–758. https://doi.org/10.1038/nature02799

Hess, S. L. G., Delamere, P., Dols, V., Bonfond, B., & Swift, D. (2010). Power transmission and particle acceleration along the Io flux tube. *Journal of Geophysical Research*, *115*(A6). https://doi.org/10.1029/2009JA014928

Hill, T. (1979). Inertial limit on corotation. *Journal of Geophysical Research*, *84*(A11), 6554. https://doi.org/10.1029/JA084iA11p06554

Hinton, P. C., Bagenal, F., & Bonfond, B. (2019). Alfvén wave propagation in the Io plasma Torus. *Geophysical Research Letters*, *46*(3), 1242–1249. https://doi.org/10.1029/2018GL081472

Hiraki, Y. (2015). Auroral vortex street formed by the magnetosphere-ionosphere coupling instability. *Annales Geophysicae*, *33*(2), 217–224. https://doi.org/10.5194/angeo-33-217-2015

Hiraki, Y., Tsuchiya, F., & Katoh, Y. (2012). Io torus plasma transport under interchange instability and flow shears. *Planetary and Space Science*, *62*(1), 41–47. https://doi.org/10.1016/j.pss.2011.11.014

Ingersoll, A. P., Vasavada, A. R., Little, B., Anger, C. D., Bolton, S. J., Alexander, C., et al. (1998). Imaging Jupiter's aurora at visible wavelengths. *Icarus*, *135*(1), 251–264. https://doi.org/10.1006/icar.1998.5971

Ivanovski, S., Kartalev, M., Dobreva, P., Vatkova, G., & Chernogorova, T. (2011). Coupled Kelvin-Helmoltz and tearing mode instabilities in the magnetopause layer. *JTAM*, *41*(3), 31–42.

Jacobsen, S., Neubauer, F. M., Saur, J., & Schilling, N. (2007). Io's nonlinear MHD-wave field in the heterogeneous Jovian magnetosphere. *Geophysical Research Letters*, *34*(10), L10202. https://doi.org/10.1029/2006GL029187

Jia, N., & Streltsov, A. V. (2014). Ionospheric feedback instability and active discrete auroral forms. *Journal of Geophysical Research: Space Physics*, *119*(3), 2243–2254. https://doi.org/10.1002/2013JA019217

Jones, S. T., & Su, Y.-J. (2008). Role of dispersive Alfvén waves in generating parallel electric fields along the Io-Jupiter fluxtube. *Journal of Geophysical Research*, *113*(A12). https://doi.org/10.1029/2008JA013512

Livengood, T. A., Moos, H. W., Ballester, G. E., & Prangé, R. M. (1992). Jovian ultraviolet auroral activity, 1981–1991. *Icarus*, *97*(1), 26–45. https://doi.org/10.1016/0019-1035(92)90055-C

Lynch, K. A., Hampton, D. L., Zettergren, M., Bekkeng, T. A., Conde, M., Fernandes, P. A., et al. (2015). MICA sounding rocket observations of conductivity-gradient-generated auroral ionospheric responses: Small-scale structure with large-scale drivers. *Journal of Geophysical Research: Space Physics*, *120*(11), 9661–9682. https://doi.org/10.1002/2014JA020860

Lysak, R. L. (1991). Feedback instability of the ionospheric resonant cavity. *Journal of Geophysical Research*, *96*(A2), 1553–1568. https://doi.org/10.1029/90JA02154

Lysak, R. L., & Song, Y. (2002). Energetics of the ionospheric feedback interaction. *Journal of Geophysical Research*, *107*(A8). https://doi.org/10.1029/2001JA000308

Lysak, R. L., & Song, Y. (2003). Kinetic theory of the Alfvén wave acceleration of auroral electrons. *Journal of Geophysical Research*, *108*(A4), 8005. https://doi.org/10.1029/2002JA009406

Mauk, B. H., Williams, D. J., & McEntire, R. W. (1997). Energy-time dispersed charged particle signatures of dynamic injections in Jupiter's inner magnetosphere. *Geophysical Research Letters*, *24*(23), 2949–2952. https://doi.org/10.1029/97GL03026

McElroy, M. B., & Yung, Y. L. (1975). The atmosphere and ionosphere of Io. *Acta Pathologica Japonica*, *196*, 227. https://doi.org/10.1086/153408

Miller, S., Tennyson, J., Geballe, T. R., & Stallard, T. (2020). Thirty years of H_3^+ astronomy. *Reviews of Modern Physics*, *92*(3), 035003. https://doi.org/10.1103/RevModPhys.92.035003

Miura, A. (1997). Compressible magnetohydrodynamic Kelvin-Helmholtz instability with vortex pairing in the two-dimensional transverse configuration. *Physics of Plasmas*, *4*(8), 2871–2885. https://doi.org/10.1063/1.872419

Miura, A., & Pritchett, P. L. (1982). Nonlocal stability analysis of the MHD Kelvin-Helmholtz instability in a compressible plasma. *Journal of Geophysical Research*, *87*(A9), 7431–7444. https://doi.org/10.1029/JA087iA09p07431

Miura, A., & Sato, T. (1980). Numerical simulation of global formation of auroral arcs. *Journal of Geophysical Research*, *85*(A1), 73–91. https://doi.org/10.1029/JA085iA01p00073

Mura, A., Adriani, A., Altieri, F., Connerney, J. E. P., Bolton, S. J., Moriconi, M. L., et al. (2017). Infrared observations of Jovian aurora from Juno's first orbits: Main oval and satellite footprints: Jovian aurora IR observations from Juno. *Geophysical Research Letters*, *44*(11), 5308–5316. https://doi.org/10.1002/2017GL072954

Mura, A., Adriani, A., Connerney, J. E. P., Bolton, S., Altieri, F., Bagenal, F., et al. (2018). Juno observations of spot structures and a split tail in Io-induced aurorae on Jupiter. *Science*, *361*(6404), 774–777. https://doi.org/10.1126/science.aat1450

Neubauer, F. (1980). Nonlinear standing Alfvén wave current system at Io: Theory. *Journal of Geophysical Research*, *85*(A3), 1171–1178. https://doi.org/10.1029/JA085iA03p01171

Nichols, J. D., & Cowley, S. W. H. (2004). Magnetosphere-ionosphere coupling currents in Jupiter's middle magnetosphere: Effect of precipitation-induced enhancement of the ionospheric Pedersen conductivity. *Annales Geophysicae*, *22*(5), 1799–1827. https://doi.org/10.5194/angeo-22-1799-2004

Nichols, J. D., & Cowley, S. W. H. (2005). Magnetosphere-ionosphere coupling currents in Jupiter's middle magnetosphere: Effect of magnetosphere-ionosphere decoupling by field-aligned auroral voltages. *Annals of Geophysics*, *23*(3), 799–808. https://doi.org/10.5194/angeo-23-799-2005

Oka, T. (1980). Observation of the infrared spectrum of H_3^+. *Physical Review Letters*, *45*(7), 531–534. https://doi.org/10.1103/PhysRevLett.45.531

Paganini, L., Villanueva, G. L., Roth, L., Mandell, A. M., Hurford, T. A., Retherford, K. D., & Mumma, M. J. (2020). A measurement of water vapour amid a largely quiescent environment on Europa. *Nature Astronomy*, *4*(3), 266–272. https://doi.org/10.1038/s41550-019-0933-6

Paranicas, C., Mauk, B., Haggerty, D., Clark, G., Kollmann, P., Rymer, A., et al. (2019). Io's effect on energetic charged particles as seen in Juno Data. *Geophysical Research Letters*, *46*(23), 13615–13620. https://doi.org/10.1029/2019GL085393

Pokhotelov, D. (2003). *Effects of the active auroral ionosphere on magnetosphere—ionosphere coupling (Thesis (Ph.D.))*. https://doi.org/10.1349/ddlp.3332

Pokhotelov, O. A., Khruschev, V., Parrot, M., Senchenkov, S., & Pavlenko, V. P. (2001). Ionospheric Alfvén resonator revisited: Feedback instability. *Journal of Geophysical Research*, *106*(A11), 25813–25824. https://doi.org/10.1029/2000JA000450

Pontius, D. H., & Hill, T. W. (1982). Departure from corotation of the Io plasma torus: Local plasma production. *Geophysical Research Letters*, *9*(12), 1321–1324. https://doi.org/10.1029/GL009i012p01321

Prangé, R., Rego, D., Southwood, D., Zarka, P., Miller, S., & Ip, W. (1996). Rapid energy dissipation and variability of the lo-Jupiter electrodynamic circuit. *Nature*, *379*(6563), 323–325. https://doi.org/10.1038/379323a0

Rankin, R., Kabin, K., Lu, J. Y., Mann, I. R., Marchand, R., Rae, I. J., & Donovan, E. F. (2005). Magnetospheric field-line resonances: Ground-based observations and modeling. *Journal of Geophysical Research*, *110*(A10), A10S09. https://doi.org/10.1029/2004JA010919

Ray, L. C., Ergun, R. E., Delamere, P. A., & Bagenal, F. (2010). Magnetosphere-ionosphere coupling at Jupiter: Effect of field-aligned potentials on angular momentum transport. *Journal of Geophysical Research*, *115*(A9). https://doi.org/10.1029/2010JA015423

Roth, L., Saur, J., Retherford, K. D., Strobel, D. F., Feldman, P. D., McGrath, M. A., & Nimmo, F. (2014). Transient water vapor at Europa's South Pole. *Science*, *343*(6167), 171–174. https://doi.org/10.1126/science.1247051

Sato, T. (1978). A theory of quiet auroral arcs. *Journal of Geophysical Research*, *83*(A3), 1042. https://doi.org/10.1029/JA083iA03p01042

Saur, J., Grambusch, T., Duling, S., Neubauer, F. M., & Simon, S. (2013). Magnetic energy fluxes in sub-Alfvénic planet star and moon planet interactions. *Astronomy & Astrophysics*, *552*, A119. https://doi.org/10.1051/0004-6361/201118179

Saur, J., Janser, S., Schreiner, A., Clark, G., Mauk, B. H., Kollmann, P., et al. (2018). Wave-particle interaction of Alfvén waves in Jupiter's magnetosphere: Auroral and magnetospheric particle acceleration. *Journal of Geophysical Research: Space Physics*, *123*(11), 9560–9573. https://doi.org/10.1029/2018JA025948

Saur, J., Strobel, D. F., & Neubauer, F. M. (1998). Interaction of the Jovian magnetosphere with Europa: Constraints on the neutral atmosphere. *Journal of Geophysical Research*, *103*(E9), 19947–19962. https://doi.org/10.1029/97JE03556

Skinner, T. E., Durrance, S. T., Feldman, P. D., & Moos, H. W. (1984). IUE observations of longitudinal and temporal variations in the Jovian auroral emission. *The Astrophysical Journal*, *278*, 441–448. https://doi.org/10.1086/161809

Streltsov, A. V., & Mishin, E. V. (2018). On the existence of ionospheric feedback instability in the Earth's magnetosphere-ionosphere system. *Journal of Geophysical Research: Space Physics*, *123*(11), 8951–8957. https://doi.org/10.1029/2018JA025942

Sulaiman, A. H., Hospodarsky, G. B., Elliott, S. S., Kurth, W. S., Gurnett, D. A., Imai, M., et al. (2020). Wave-particle interactions associated with Io's auroral footprint: Evidence of Alfvén, ion cyclotron, and whistler modes. *Geophysical Research Letters*, *47*. https://doi.org/10.1029/2020GL088432

Szalay, J. R., Allegrini, F., Bagenal, F., Bolton, S. J., Bonfond, B., Clark, G., et al. (2020a). Alfvénic accelerationsustains Ganymede's footprint tail aurora. *Geophysical Research Letters*, *47*(3), e2019GL086527. https://doi.org/10.1029/2019GL086527

Szalay, J. R., Allegrini, F., Bagenal, F., Bolton, S. J., Bonfond, B., Clark, G., et al. (2020b). A new framework to explain changes in Io's footprint tail electron fluxes. *Geophysical Research Letters*, *47*(18), e2020GL089267. https://doi.org/10.1029/2020GL089267

Szalay, J. R., Bagenal, F., Allegrini, F., Bonfond, B., Clark, G., Connerney, J. E. P., et al. (2020). Proton acceleration by Io's Alfvénic Interaction. *Journal of Geophysical Research: Space Physics*, *125*(1), e2019JA027314. https://doi.org/10.1029/2019JA027314

Thomas, N., Bagenal, F., Hill, T. W., & Wilson, J. K. (2004). The Io neutral clouds and plasma torus. In F. Bagenal, T. E. Dowling, & W. B. McKinnon (Eds.), *Jupiter. The planet, satellites and magnetosphere* (Vol. 1, pp. 561–591). Cambridge University Press.

Thomas, N., Lichtenberg, G., & Scotto, M. (2001). High-resolution spectroscopy of the Io plasma torus during the Galileo mission. *Journal of Geophysical Research*, *106*(A11), 26277–26291. https://doi.org/10.1029/2000JA002504

Trafton, L., Carr, J., Lester, D., & Harvey, P. (1989). *Jupiter's Aurora: Detection of quadrupole h2 emission* (p. 494). NASA Special Publication.

Tulegenov, B., & Streltsov, A. V. (2017). Ionospheric Alfvén resonator and aurora: Modeling of MICA observations. *Journal of Geophysical Research: Space Physics*, *122*(7), 7530–7540. https://doi.org/10.1002/2017JA024181

Vasavada, A. R., Bouchez, A. H., Ingersoll, A. P., Little, B., & Anger, C. D. (1999). Jupiter's visible aurora and Io footprint. *Journal of Geophysical Research*, *104*(E11), 27133–27142. https://doi.org/10.1029/1999JE001055

von Kármán, T. (1911). Ueber den Mechanismus des Widerstandes, den ein bewegter Körper in einer Flüssigkeit erfährt. *Nachrichten von der Gesellschaft der Wissenschaften zu Göttingen, Mathematisch-Physikalische Klasse*, 509–517.

Watanabe, H., Kita, H., Tao, C., Kagitani, M., Sakanoi, T., & Kasaba, Y. (2018). Pulsation characteristics of Jovian infrared Northern aurora observed by the Subaru IRCS with adaptive optics. *Geophysical Research Letters*, *45*(21), 11,547–11,554. https://doi.org/10.1029/2018GL079411

Watanabe, T.-H. (2010). Feedback instability in the magnetosphere-ionosphere coupling system: Revisited. *Physics of Plasmas*, *17*(2), 022904. https://doi.org/10.1063/1.3304237

Wu, W., Peng, S., Ma, T., Ren, H., Zhang, J., Zhang, T., et al. (2019). Status of high current H_2^+ and H_3^+ ion sources. *Review of Scientific Instruments*, *90*(10), 101501. https://doi.org/10.1063/1.5109240